Journal of Solid State Chemistry 210 (2014) 171–177

Contents lists available at ScienceDirect

Journal of Solid State Chemistry

journal homepage: www.elsevier.com/locate/jssc

TiO_2 synthesized by microwave assisted solvothermal method: Experimental and theoretical evaluation

K.F. Moura [a], J. Maul [a], A.R. Albuquerque [a], G.P. Casali [a], E. Longo [b], D. Keyson [a], A.G. Souza [a], J.R. Sambrano [c], I.M.G. Santos [a,*]

[a] INCTMN/LACOM, Departamento de Química, Universidade Federal da Paraíba, Campus 1, CEP 58059-900 João Pessoa, PB, Brazil
[b] INCTMN/LIEC, Instituto de Química, Universidade Estadual Paulita, Rua Prof. Francisco Degni, 55, Quitandinha, CEP 14800-900 Araraquara, SP, Brazil
[c] INCTMN/LSM, Departamento de Matemática, Universidade Estadual Paulista, Av. Eng. Luiz Edmundo Carrijo Coube, 14-01, CEP 17033-360 Bauru, SP, Brazil

ARTICLE INFO

Article history:
Received 26 March 2013
Received in revised form
12 November 2013
Accepted 16 November 2013
Available online 23 November 2013

Keywords:
TiO_2
Nanoparticles
Microwave solvothermal synthesis
Computational periodic model
B3LYP-D*

ABSTRACT

In this study, a microwave assisted solvothermal method was used to synthesize TiO_2 with anatase structure. The synthesis was done using Ti (IV) isopropoxide and ethanol without templates or alkalinizing agents. Changes in structural features were observed with increasing time of synthesis and evaluated using periodic quantum chemical calculations. The anatase phase was obtained after only 1 min of reaction besides a small amount of brookite phase. Experimental Raman spectra are in accordance with the theoretical one. Micrometric spheres constituted by nanometric particles were obtained for synthesis from 1 to 30 min, while spheres and sticks were observed after 60 min.

1. Introduction

Nanocrystalline titanium dioxide (TiO_2) has recently attracted significant attention for scientific and technological applications in electronic and optical–electronic devices, catalysts, gas sensors and semiconductors for solar cells [1,2]. TiO_2 is a polymorphic material with three distinct crystallographic structures: tetragonal anatase, orthorhombic brookite and tetragonal rutile [3]. The thermodynamic stability of TiO_2 structures depends on particle size: anatase is the most thermodynamically stable structure of TiO_2 at particle sizes up to 11 nm, brookite is the most stable structure between 11 and 35 nm, and rutile is the most stable structure above 35 nm [4]. In addition, the material properties of TiO_2 depend on the method of synthesis; TiO_2 synthesis can be performed using sol–gel [5], thermal evaporation [6], co-precipitation [7], micro-emulsion [8] and hydrothermal/solvothermal methods [9]. The hydrothermal and solvothermal methods have particularly been of increasing interest recently due to the possibility of obtaining crystalline metallic oxides with high purity and morphological control [10,11]. Most papers regarding these techniques are related to the evaluation of pressure, temperature and use of templates [12–15]. Lee et al. [16] reported the synthesis of anatase (TiO_2) spheres in ethanolic media using tetrabutylammonium hydroxide (TBAH, 40% aqueous solution) as template at 200 °C for 6 h of microwave exposure. Du et al. [17] obtained TiO_2 anatase microspheres using aqueous $TiCl_4$, sodium sulfate (Na_2SO_4), urea $CO(NH_2)_2$ and ethanol above 140 °C with reaction times ranging from 1 to 36 h. The microwave method has also been used to obtain TiO_2 microspheres by Luo et al. [18], Yoon et al. [19] and Jia et al. [20]. Luo et al. [18] used NaOH as an alkalinizer and sodium dodecyl sulfonate (SDS) as template in ethanolic media at 140 °C and a reaction time of 40 min. Yoon et al. [19] studied the formation of TiO_2 from $TiCl_4$ and $TiCl_3$ in a 20% HCl aqueous solution at 190 °C for 30 min and evaluated the influence of the alcohol chain length in the solution on the morphology of the material. Jia et al. [20] prepared TiO_2 sticks using $TiCl_4$ as a precursor in addition to polyethyleneoxide–polypropyleneoxide–polyethyleneoxide copolymer in HCl with further heat treatment at 300 °C. TiO_2 microspheres with rutile structures were also obtained by Mali et al. in two different studies. In 2012 [21], Mali et al. synthesized TiO_2 films containing microspheres using the hydrothermal method. Semi-spheres were obtained after 4 h at 160 °C, and perfect spheres were obtained after 6 h. In 2013 [22], Mali et al. improved the light harvesting of films obtained after 8 h of hydrothermal treatment by deposition of CdS on the surface of the microspheres using the successive ionic layer adsorption and reaction (SILAR) technique.

In this study, TiO_2 microspheres were synthesized using the microwave assisted solvothermal method without the use of a template or the previously reported alkalinizing agents and with reaction times ranging from 1 to 60 min. Periodic quantum

* Corresponding author. Tel./fax: +55 83 32167441.
E-mail addresses: ieda@quimica.ufpb.br, ieda.garcia@pq.cnpq.br (I.M.G. Santos).

0022-4596/$ - see front matter © 2013 Elsevier Inc. All rights reserved.
http://dx.doi.org/10.1016/j.jssc.2013.11.023

chemical calculations were performed to evaluate the dependence of the vibrational normal modes on the structural order–disorder and on the lattice parameters.

2. Materials and methods

2.1. Experimental procedure

For the synthesis of titanium dioxide (TiO_2) particles, an ethanolic suspension with 0.07 mol L^{-1} of Ti(IV) was prepared using Ti(IV) isopropoxide (Aldrich, 97% purity) and ethanol (Vetec, 99.8%) under continuous stirring. This suspension was transferred to a Teflon reactor and heated by microwave radiation at 120 °C under autogenic pressures of approximately 200 kPa, for reaction times of 1, 5, 15, 30 and 60 min. A white precipitate was formed during the reaction; after the reaction was completed, this precipitate was washed with distilled water at room temperature until complete neutralization. The precipitate was dried at 100 °C for 5 h.

Characterization was performed using X-ray diffraction (XRD) in an XRD 6000 Shimadzu diffractometer using Cu*K*α radiation. Identification was performed comparing XRD patterns with the crystallographic index cards JCPDS 89-4921, 89-4920 and 38-0700. Crystallite size was calculated using the Scherrer equation for the (101) peak. Raman spectra were obtained using an FT-Raman Bruker RFS/100/S spectrophotometer with a 60-mW Nd:YAG laser, excitation radiation of 1064 nm and a resolution of 4 cm^{-1} between 50 and 750 cm^{-1}. Infrared spectra between 400 and 1500 cm^{-1} were obtained with an IRPrestige-21 Shimadzu spectrometer. Morphological evaluation was performed using FE-SEM in a FEG-VP Zeiss Supra 35 microscope.

TiO_2 samples were tested for the photodegradation of Remazol Golden Yellow (RNL) azo-dye. A 5-mg aliquot of the TiO_2 sample prepared using a 1-min reaction time was added to a 50-ppm RNL solution of pH = 6, and the resulting mixture was submitted to UVC radiation (0.5–1 mW measured near the sample) for 1, 2 or 4 h. The solution was then centrifuged for 30 min at 5000 rpm and 25 °C to separate the solution from the catalyst via filtration. The discoloration of the solutions was analyzed by UV–vis spectroscopy using a SHIMADZU UV-2550, in the range of 200–600 nm.

2.2. Computational details

To evaluate the dependence of vibrational normal modes on lattice parameters, the anatase structure was explored by computational quantum calculations, and a relationship between the blue-shift/red-shift of vibrational modes and crystal growth was found. Our ansatz was δ (time of synthesis)→δ (crystallization degree)→δ (lattice parameters)→blue-shift/red-shift. For this analysis, periodic DFT calculations were performed with the B3LYP hybrid functional as implemented in CRYSTAL09 computer code [23], which uses a local Gaussian basis set to describe crystalline orbitals.

The anatase phase was modeled with a conventional unit cell composed of four units of TiO_2 (two primitive cells belonging to the space group $I4_1/amd$), defined by three crystallographic parameters: *a*, *c* and internal coordinate *u* ($u = d_{ap}/c$, where d_{ap} is the apical Ti–O bond length). The oxygen and titanium centers were described by the all-electron basis set: 6-31G* for O and 6-21(*d*-31)G for Ti. The Grimme dispersion potential was included to improve the structural description of anatase using the augmented B3LYP-D* method, as reported in Ref. [24].

Values of 10^{-8}, 10^{-8}, 10^{-8}, 10^{-8} and 10^{-18} for the tolerances controlling Coulomb and exchange series were adopted for all calculations. The shrinking factor (Pack–Monkhorst and Gilat net) was set to 6, corresponding to 40 independent *k*-points in the irreducible part of the Brillouin zone integration. The exchange and correlation functionals were integrated numerically on a grid of points. The SCF criteria convergence was 10^{-7}, 10^{-10} and 10^{-8} for the geometry optimizations, vibrational and EOS calculations, respectively.

To evaluate the order–disorder degree in TiO_2 anatase, all structural parameters were optimized at 10 fixed volumes (*V*) in the range $0.92 < V/V_0 < 1.08$, where V_0 is the equilibrium unit cell volume, using the EOS (Equation of States) algorithm.

Analyses of the infrared and Raman normal modes and their corresponding frequencies for all optimized bulks were computed at the Γ point by diagonalizing the mass-weighted Hessian matrix. For this step, the functionals B3PW-D and PBE0-D with default van der Waals radii in the Grimme potential [25] were also applied.

All calculations were performed in a high performance computer center or in an in-house Linux cluster using the parallel version of CRYSTAL09. The graphical manipulations were performed using the molecular graphics programs MOLDRAW and VESTA for Microsoft Windows [26–28].

3. Results and discussion

FE-SEM micrographs of the TiO_2 samples are presented in Fig. 1. The presence of spheres formed by agglomerated nanometric particles with sizes varying from 35 to 50 nm was observed. For reaction times of 1–30 min, spheres of 1-μm average diameter were observed (Fig. 2). Coalescence and misshaped spheres were observed even after a 1-min reaction time, but were more evident after 30 min. For 60-min reaction times, spheres and sticks that varied in size were observed, indicating that microwave treatment has an important influence on the material morphology.

The most important difference between the present study and the previous literature on microspheres produced by hydrothermal/solvothermal methods [16–20] is that the synthesis of TiO_2 microspheres is performed without templates or alkalinizing agents. In addition, this TiO_2 microparticle synthesis was completed in a very short reaction time (1 min).

The crystalline structures of the TiO_2 samples prepared at different reaction times were characterized by XRD, as shown in Fig. 3. All of the samples crystallized into the anatase structure and a small amount of brookite as secondary phase. Peaks related to rutile or hydroxides were not observed even for 1-min reaction times. No further thermal treatments or the use of templates was necessary, as observed in previous literature reporting the synthesis of TiO_2 by this method [29].

The structure of anatase is tetragonal with the space group D_{4h}^{19} $I4_1/amd$ and is formed by Ti^{4+} ions at the center of octahedra.

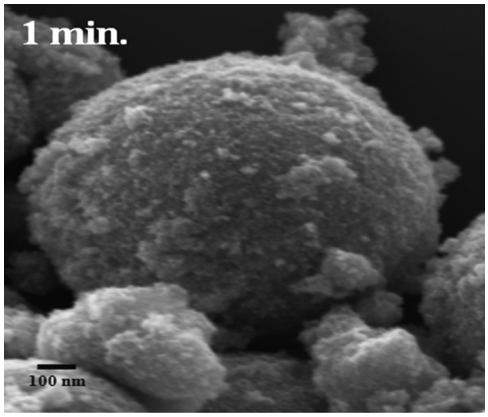

Fig. 1. FE-SEM micrograph of TiO_2 obtained with 1 min of synthesis.

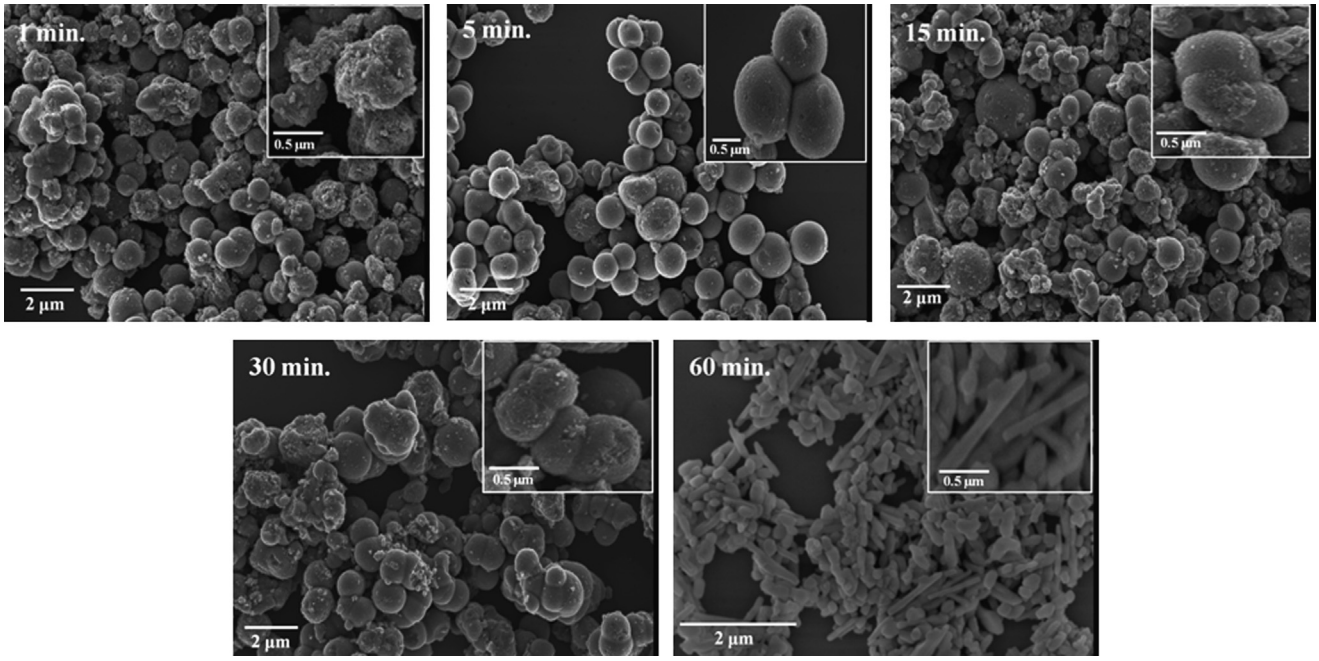

Fig. 2. FE-SEM micrographs of TiO_2 obtained with different durations of synthesis.

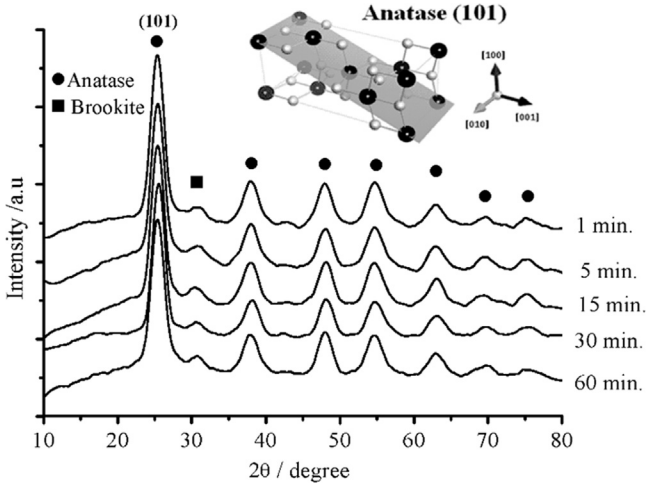

Fig. 3. XRD patterns of TiO_2 prepared using different durations of synthesis. The inset shows the (101) plane of anatase unit cell, used to obtain geometric parameters.

Brookite has an orthorhombic structure with the space group D_{2h}^{15} *Pbca*, presenting a higher density than that of anatase with higher distortions in the Ti^{4+} octahedra; bond length and angles are slightly different from one another, leading to a loss in the C_1 local symmetry [30]. Various studies have evaluated the crystallization behavior of the anatase and brookite structures. According to Zhao et al. [31], different mechanisms of crystallization occur when synthesis is performed using the hydrothermal method. The crystal growth of anatase follows Ostwald's ripening mechanism with the formation of $[Ti(OH)_2(OH_2)_4]^{2+}$ under acidic or near neutral conditions. The crystal growth of brookite begins with the formation of TiO_6 octahedra in an alkaline solution followed by Ostwald's step rule. In the present work, the synthesis is performed under pH ≈ 4–5, favoring the crystallization of anatase. We believe that brookite formation may be related to the heterogeneity of the solution due to the crystallization process, as no stirring is performed during solvothermalization and the ionic mobility is smaller when ethanol is used as solvent instead of water.

Table 1
Characteristics of the samples according to the XRD patterns.

	Time (min)				
	1	**5**	**15**	**30**	**60**
FWHM of the (101) peak (deg)	1.43	1.31	1.04	0.95	0.82
Lattice parameter ***a*** (Å)	3.80	3.78	3.81	3.80	3.80
Lattice parameter ***c*** (Å)	9.51	9.41	9.42	9.49	9.56
Unit cell volume (Å^3)	137	134	137	137	138
Crystallite size (Å)	57.0	62.0	78.5	85.8	100

The lattice parameters, unit cell volume, full width at half maximum of the peak (FWHM) and crystallite sizes are presented in Table 1. The evaluation of these results indicates that an increase in the reaction time leads to a decrease in the width of the (101) XRD peak, due to a higher long range order related to the increase in the crystallite size. This result indicates that processes of dissolution–recrystallization are not important for this synthesis. Evaluation of the lattice parameters indicates that the *a* values are almost constant, while an increase in the *c* value is observed for reaction times longer than 1 min. Huberty and Xu [32] previously reported that the *c* parameter of anatase decreased upon an increase in the amount of brookite due to the presence of microstrain in the anatase induced by brookite attachment. Other factors, including structural defects, dopants, synthesis route and microstrains, may also affect this parameter.

The short-range order of the anatase is evaluated by infrared and Raman spectroscopy, shown in Fig. 4. According to the group theory, the anatase structure (space group D_{4h}^{19}) has three acoustic modes and 15 optical modes. Among these optical modes, the irreducible representations are as follows: $1A_{1g}+1A_{2u}+2B_{1g}+1B_{2u}+3E_g+2E_u$. Representations with the subscript *u* are infrared active while representations with the subscript *g* are Raman active. The B_{2u} mode is silent [33].

The infrared spectra are shown in Fig. 4a and b; TiO_2 with anatase structure presents three infrared active vibrational modes,

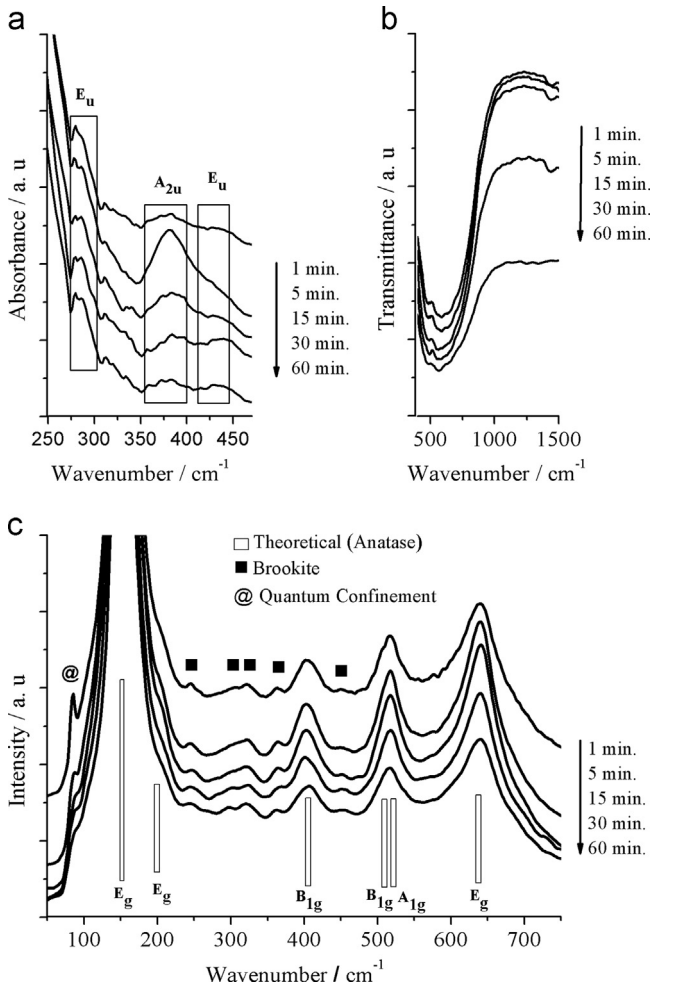

Fig. 4. Spectra of TiO_2 prepared using different periods of time. (a) Absorbance infrared spectra in the far region. (b) Transmittance infrared spectra in the medium region. (c) Raman spectra.

Table 2
Theoretical and experimental infrared (IR) and Raman (R) modes and their irreducible representations for relaxed TiO_2 anatase (T=25 °C and p=1 atm).

Modes	B3LYP-D*[a]	B3PW-D[b]	PBE0-D[c]	Exp	This work[d]	Active
E_g (2)	136	122	121	143 [33]	149–151	R
E_g (2)	187	190	194	198 [33]	203–207	R
E_u (2)	207	191	195	262 [34]	273–275	IR
A_{2u}	329	319	322	367 [34]	365–390	IR
B_{1g}	424	415	416	395 [33]	403–407	R
E_u (2)	432	420	421	435 [34]	430–445	IR
B_{1g}	512	504	507	512 [33]	515–517	R
A_{1g}	524	517	518	518 [33]	515–517	R
B_{2u}	559	553	556	–	–	Silent
E_g (2)	638	625	627	639 [33]	630–641	R

[a] Optimization using B3LYP-D*, frequencies using B3LYP-D* [24].
[b] Optimization using B3LYP-D*, frequencies using B3PW-D.
[c] Optimization using B3LYP-D*, frequencies using PBE0-D.
[d] Interval for t=1–60 min.

$2E_u+A_{2u}$ [29]. In the present study, broad bands assigned to these three modes were observed at approximately 280 cm^{-1} (E_u), 380 cm^{-1} (A_{2u}) and 440 cm^{-1} (E_u) (Fig. 4a) in addition to superposed bands between 400 and 900 cm^{-1} (E_u and A_{2u}) (Fig. 4b), which is in agreement with other experimental data [34]. The presence of the brookite phase is characterized by broad bands at approximately 764 and 806 cm^{-1} [35], which were not observed in the present study, most likely due to the low amount of this phase and superposition with anatase bands.

All Raman spectra (Fig. 4c) of the TiO_2 synthesized in this study presented the modes $1A_{1g}+2B_{1g}+3E_g$ at 149–151 cm^{-1} (E_g), 203–207 cm^{-1} (E_g), 403–407 cm^{-1} (B_{1g}), 515–517 cm^{-1} (B_{1g}/A_{1g}) and 630–641 cm^{-1} (E_g), in addition to weak bands at 247, 322, 362, 454, 461 and 588 cm^{-1} relative to the brookite phase [36]. Moreover, one mode at 86 cm^{-1} was observed and assigned to vibrations characteristic of small crystallites, most likely from particle surface and quantum confinement, which tends to disappear when the reaction time and crystallite size increase [37]. Experimental results for single crystal anatase indicate that these modes are usually observed at 143 cm^{-1} (E_g), 198 cm^{-1} (E_g), 395 cm^{-1} (B_{1g}), 512 cm^{-1} (B_{1g}), 518 cm^{-1} (A_{1g}) and 639 cm^{-1} (E_g) [38]. Previous literature and the present work indicate that a blue-shift occurs at 639 cm^{-1}, with the exception of the E_g mode. A difference in the behavior of this mode was also observed by Ohsaka [39], who evaluated the dependence of the Raman spectrum of anatase on temperature. The blue-shift phenomenon is usually present in nanometric anatase [40,41]. For nanometric materials, the surface tension may exert a radial pressure on the nanocrystal, which may act in a manner similar to the effect of hydrostatic pressure on single crystals and lead to the frequency upshift of the E_g anatase mode at 143 cm^{-1} [42].

In the present work, the influence of pressure on the anatase structure is simulated using computational quantum calculations. The simulated anatase structure (a=3.7875 Å, c=9.5146 Å, and u=0.2082—as previously reported in Ref. [24]) at the B3LYP-D* level is in excellent agreement with the single crystal experimental data (a=3.7842 Å, c=9.5146 Å, and u=0.2081). Theoretical infrared and Raman vibrational modes were computed at the Γ point using B3LYP-D*, B3PW-D and PBE0-D functionals with the optimized relaxed structure obtained from the B3LYP-D* at 25 °C and 1 atm and are displayed in Table 2.

The positions of all estimated vibrational modes were similar to those of the experimental modes, but several small deviations between the modes occurred due to the nature of the calculation level. Despite these small deviations, the qualitative analysis of the vibrational modes and their behavior in relation to the expansion/compression simulation of a unit cell is useful for discussion of the order–disorder model.

According to the theoretical calculation performed in this work, all of the E_g and E_u vibrations occur in the [100] and [010] directions and are doubly degenerated as a consequence of having a tetragonal structure, which has the lattice parameter a equal to b but different from c. The E_g mode at approximately 149 cm^{-1} is mostly related to the Ti^{4+} vibration inside the TiO_6 octahedra—[TiO_6], with a smaller contribution of the O^{2-} ions. The E_g mode at 642 cm^{-1} is mostly due to the movement of the O^{2-} anions between two octahedra—[TiO_6–TiO_6] octahedral deformations. The A and B vibrations are in the [001] direction, indicating the stretching of Ti–O–Ti bonds.

The influence of the lattice parameters on the theoretical vibrational spectra was analyzed (Fig. 5). Compression (related to a decrease in lattice parameters) led to a decrease in the apical (d_{ap}) and equatorial (d_{eq}) distances of the Ti–O bonds and the θ_2 angle (Ti–O–Ti). All of the vibrational modes increased in wavenumber (blue-shift) upon a decrease in the lattice parameter c and, consequently, the unit cell volume, which is directly related to the increase in the pressure. The only exception was E_g ($\sim$187 cm^{-1}), which presented a small red-shift behavior for $c>9.40$ Å. Ohsaka [43] evaluated the effect of the hydrostatic pressure on the Raman spectrum of anatase and observed the same behavior for the E_g and B_{1g} modes, as reported in our work.

With regard to the experimental data, a random behavior was observed in the position of the Raman modes in relation to the

lattice parameters, with the exception of the E_g mode at 639 cm^{-1}. This mode was selected to evaluate the correlation between the theoretical and the experimental data as a function of the *c* lattice parameter (Fig. 6). The experimental values converge to the theoretical values upon an increase in crystallite size, as a result of the increase in the ratios of bulk/surface and bulk/interface. The highest agreement between theoretical and experimental results was obtained for samples with 60-min reaction times and crystallite sizes of approximately 100 nm, leading to properties more similar to the bulk properties simulated in the periodic model.

In the Raman spectra of single crystal anatase, the experimental data of the E_g mode at 639 cm^{-1} shows a red-shift in relation to the lattice parameter '*c*'. This result is confirmed by comparing the theoretical results and experimental data, which indicates that samples with lower lattice parameter '*c*' values (corresponding to smaller crystallite sizes) showed a higher red-shift in relation to the theoretical results, as shown in Fig. 6. The global changes in the primitive unit cell of the anatase structure indicate that the distance between oxygen anions increases as the lattice parameter decreases due to the compression effect. Because the E_g mode at 639 cm^{-1} is related to the movement of these anions in opposite directions, a higher energy would be necessary to promote this vibration. The experimental data indicate that there is a limit on increasing this energy, which may be assigned to some short-range disorder.

The short-range disorder is evaluated using the bandwidth of the Raman modes at 149 cm^{-1}, 402 cm^{-1} and 642 cm^{-1}, as shown in Table 3. These are the most intense bands of the Raman spectra and are not superimposed with other modes.

The foundations of the presented order–disorder model are supported by the observation that in the TiO_2 nanophase, the size-induced radial pressure may act in a manner similar to the effect of hydrostatic pressure on single crystals [44]. Although the simple model described herein does not consider the full extent of the crystal growth process, it does reveal some structural order–disorder effects.

Analysis of the data presented in Table 3 indicates an increase in the FWHM of 149 cm^{-1} and 642 cm^{-1} modes in addition to a decrease in the 402 cm^{-1} mode as the reaction time increases. Evaluation of these results involves considering the theoretical calculations. As the E_g mode at 149 cm^{-1} is related to the movement of the Ti^{4+} vibration in the [100] direction, this increase indicates that a higher short-range disorder occurs inside the octahedra as the reaction time increases. Moreover, the short-range disorder also increases between octahedra as indicated by the (Ti–O–Ti) vibration evaluated in the E_g mode at 642 cm^{-1} for the sample obtained after a 60-min reaction time. This higher short-range disorder can be credited to the observation that the anatase phase decreases in stability as the crystallite size increases, as reported by Chen et al. [4]. In the [001] direction, a decrease in the short-range disorder is indicated by the B_{1g} mode, which may be related to the increase in the lattice parameter *c*.

The microspheres obtained after 1-min reaction times were tested for the photocatalytic degradation of the RNL azo-dye (Fig. 7). The photocatalyst synthesized in the present work showed an increase in efficiency indicated by an increase in the discoloration of the azo-dye as exposure to UV radiation increased. Comparison with the P25 TiO_2 showed a difference of 14%. This efficiency may be due to the smaller particle size and/or the presence of brookite; Zhao et al. [31] showed that the concomitant presence of two phases might increase the catalytic activity due to the easier transfer of photogenerated electrons from one phase to another, suppressing the recombination process.

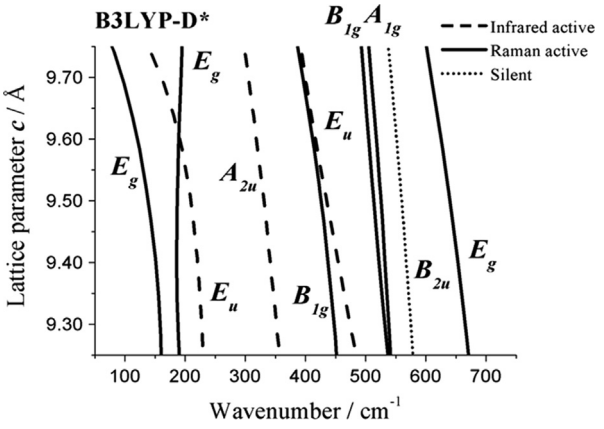

Fig. 5. Theoretical vibrational spectra of TiO_2 at different values of *c* lattice parameter calculated at B3LYP-D* level.

4. Conclusions

The microwave-assisted solvothermal method was successfully used in the synthesis of titanium dioxide with anatase structure without further thermal treatment when using 1- to 60-min reaction times. The long-range order increased with increasing reaction time while the short-range disorder increased in the [100] direction and decreased in the [001] direction. The band indicating

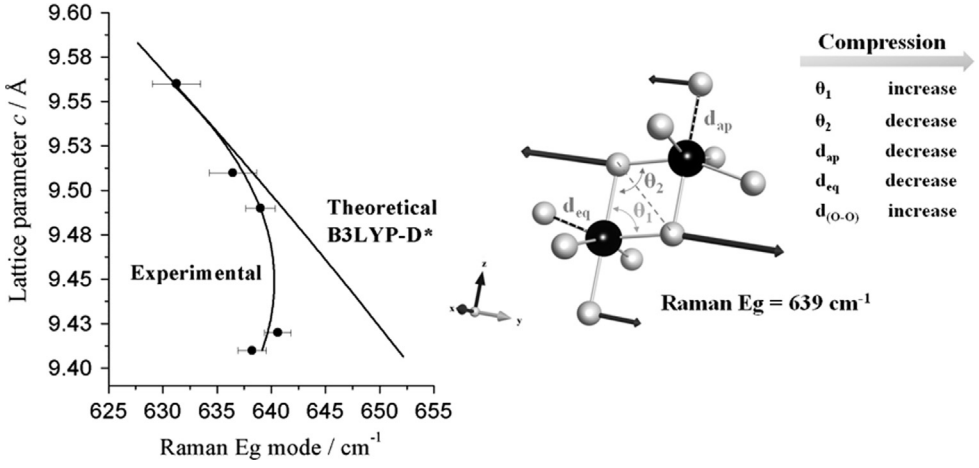

Fig. 6. Variation in the position of the theoretical and experimental E_g modes in the Raman spectra of TiO_2 at different values of *c* lattice parameter and its vector displacements on the primitive unit cell.

Table 3
FWHM of the Raman peaks.

Time (min)	E_g=149 cm^{-1}	R^2	B_{1g}=402 cm^{-1}	R^2	E_g=642 cm^{-1}	R^2
1	18.90	0.999	23.40	0.998	32.10	0.998
5	18.95	0.999	23.40	0.998	32.10	0.999
15	21.50	0.998	23.40	0.998	32.14	0.999
30	21.65	0.998	18.75	0.999	34.05	0.999
60	22.56	0.998	17.40	0.998	37.80	0.998

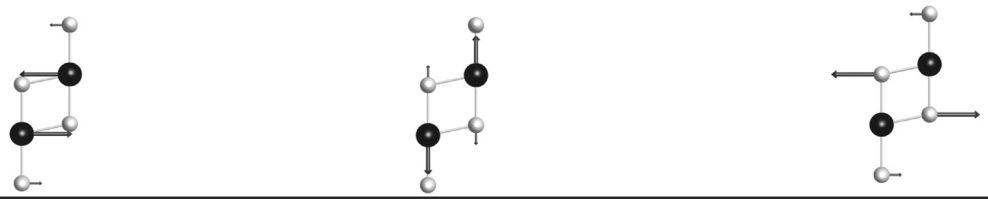

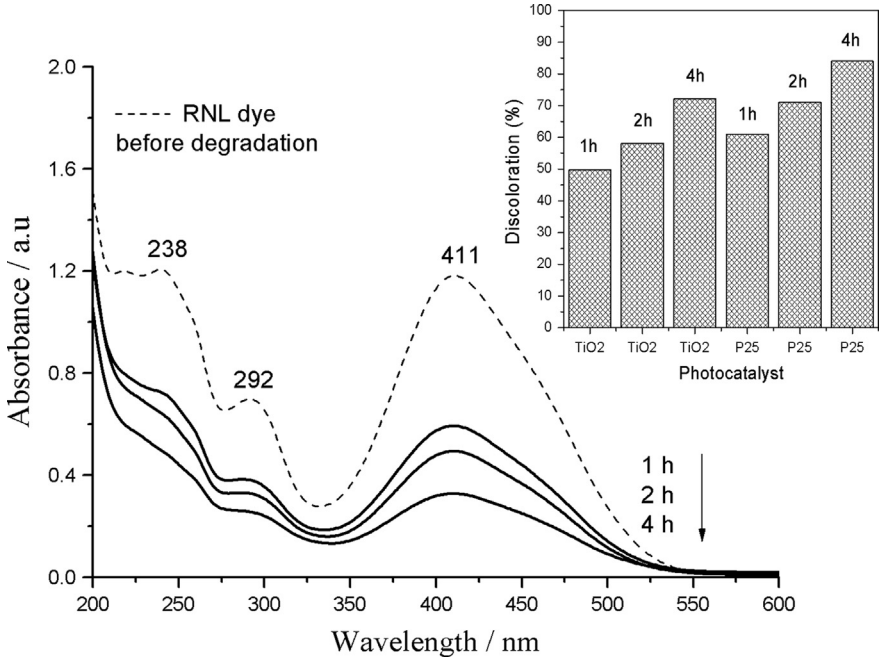

Fig. 7. Results of discoloration of the samples submitted to photodegradation.

quantum confinement was more intense using a 1-min reaction time sample. As shown in the FE-SEM micrographs, the nanometric particles agglomerate to form microspheres in reaction times of up to 30 min, but a change in the morphology occurs when a 60-min reaction time is used.

Computational studies based on periodic DFT computations were important for elucidating vibrational behavior regarding the proposed order–disorder model. The experimental Raman and FT-IR modes are in close agreement with the theoretical results, particularly in supporting the observation that an increase in the reaction time results in an increase in the crystallite size.

The photocatalytic tests showed that TiO_2 synthesized in the present work led to a discoloration of 72.2% after a 4-h reaction time.

Acknowledgments

This work is supported by Brazilian Funding Agencies FAPESP, CAPES, CNPq and INCTMN-Unesp-UFPB. Computer facilities were supported by resources supplied by the Molecular Simulation Laboratory and the Center for Scientific Computing of the São Paulo State University.

References

[1] B. O'regan, M. Grätzel, Nature 353 (1991) 737–740.
[2] T. Watanabe, H. Hayashi, H. Imai, Sol. Energy Mater. Sol. Cells 90 (2006) 640–648.
[3] J. Beusen, M.K. Van Bael, H. Van den Hul, J. D'haen, J. Mullens, J. Eur. Ceram. Soc. 27 (2007) 4529–4535.
[4] B. Chen, H. Zhang, K.A. Dunphy, D. Spagnoli, M.B. Kruger, D.V.S. Muthu, M. Kunz, S. Fakra, J.Z. Hu, Q.Z. Guo, J.F. Banfield, Phys. Rev. B 79 (2009) 125406.
[5] K. Prasad, D.V. Pinjari, A.B. Pandit, S.T. Mhaske, Ultrason. Sonochem. 17 (2010) 409–415.
[6] Y. Yu, J. Wang, J.F. Parr, Proc. Eng. 27 (2012) 448–456.
[7] G. Mouret, K. Mozet, H. Muhr, E. Plasari, M. Martin, Powder Technol. 190 (2009) 84–88.
[8] W. Bauer, G. Tomandl, Ceram. Int. 20 (1994) 189–193.
[9] S.S. Mali, P.S. Shinde, C.A. Betty, P.N. Bhosale, W.J. Lee, P.S. Patil, Appl. Surf. Sci. 257 (2011) 9737–9746.
[10] S.A. Borkar, S.R. Dharwadkar, Ceram. Int. 30 (2004) 509–514.
[11] S.W. Oh, S.H. Park, Y.K. Sun, J. Power Sources 161 (2006) 1314–1318.

[12] Q. Zhang, W. Li, S. Liu, Powder Technol. 212 (2011) 145–150.
[13] L. Lei, C. Yuming, L. Bo, Z. Xingfu, D. Weiping, Appl. Surf. Sci. 256 (2010) 2596–2601.
[14] Y. Zhang, J. Zhang, P. Wang, G. Yang, Q. Sun, J. Zheng, Y. Zhu, Mater. Chem. Phys. 123 (2010) 595–600.
[15] H.W. Wang, C.H. Kuo, H.C. Lin, I.T. Kuo, C.F. Cheng, J. Am. Ceram. Soc. 89 (2006) 3388–3392.
[16] H. Lee, M. Choi, Y. Kye, M. An, I.M. Lee, Bull. Korean Chem. Soc. 33 (5) (2012) 1699.
[17] J. Du, W. Chen, C. Zhang, Y. Liu, C. Zhao, Y. Dai, Chem. Eng. J. 170 (2011) 53–58.
[18] H.L. Luo, J. Sheng, Y.Z. Wan, Mater. Lett. 62 (2008) 37–40.
[19] S. Yoon, E.S. Lee, A. Manthiram, Inorg. Chem. 51 (2012) 3505–3512.
[20] X. Jia, W. He, X. Zhang, H. Zhao, Z. Lil, Y. Feng, Nanotechnology 18 (2007) 075602, http://dx.doi.org/10.1088/0957-4484/18/7/075602.
[21] S.S. Mali, C.A. Betty, P.N. Bhosale, P.S. Shinde, M.R. Pramod, S.R. Jadkar, P.S. Patil, CrystEngComm 14 (2012) 8156–8161.
[22] S.S. Mali, R.S. Devan, Y. Ma, C.A. Betty, P.N. Bhosale, R.P. Panmand, B.B. Kale, S.R. Jadkar, P.S. Patil, J. Kimg, C.K. Hong, Electrochim. Acta 90 (2013) 666–672.
[23] R. Dovesi, V.R. Saunders, C. Roetti, R. Orlando, C.M. Zicovich-Wilson, F. Pascale, B. Civalleri, K. Doll, N.M. Harrison, I.J. Bush, P. D'Arco, M. Llunell, Proceedings of CRYSTAL09, Torino, 2009.
[24] A.R. Albuquerque, M.L. Garzim, I.M.G. dos Santos, V. Longo, E. Longo, J.R. Sambrano, J. Phys. Chem. A 116 (2012) 11731–11735.
[25] G. Dierker, G. Kehr, R. Fröhlich, G. Erker, S. Grimme, J. Comput. Chem. 27 (2006) 1787–1799.
[26] C. Pisani, Lecture Notes in Chemistry, vol. 67, Spinger Verlag, Heidelberg, 1996.
[27] R. Dovesi, B. Civalleri, R. Orlando, C. Roetti, Rev. Comput. Chem. 21 (2005) 1–125.
[28] P. Ugliengo, G. Borzani, J. Appl. Crystallogr. 21 (1988) 75.
[29] M. Horprathum, P. Eiamchai, P. Chindaudom, A. Pokaipisitb, P. Limsuwan, Proc. Eng. 32 (2012) 676–682.
[30] M. Landmann, E. Rauls, W.G. Schmidt, J. Phys.: Condens. Matter 24 (2012) 195–503.
[31] B. Zhao, L. Lin, D. He, J. Mater. Chem. A 1 (2013) 1659.
[32] J. Huberty, H. Xu, J. Solid State Chem. 181 (2008) 508–514.
[33] M.J. Šćepanović, M. Grujić-Brojčin, Z.D. Dohčević-Mitrović, Z.V. Popović, Sci. Sintering 23 (2003) 691–696.
[34] M. Giarola, A. Sanson, F. Monti, G. Mariotto, M. Bettinelli, A. Speghini, G. Salviulo, Phys. Rev. B 81 (2010) 7.
[35] A. Verma, S.B. Samanta, A.K. Bakhshib, S.A. Agnihotry, Sol. Energy Mater. Sol. Cells 88 (2005) 47–64.
[36] Ü.Ö.A. Arıer, F.Z. Tepehan, Surf. Coat. Technol. 206 (2011) 37–42.
[37] A. Gajovic, M. Stubicar, M. Ivanda, K. Furic, J. Mol. Struct. 563–564 (2001) 315–320.
[38] M. Horn, C.F. Schwerdt, E.P. Meagher, Z. Kristallogr. 136 (1972) 273.
[39] T. Ohsaka, J. Phys. Soc. Jpn. 48 (1980) 1661–1668.
[40] R.J. Gonzalez, R. Zallen, H. Berger, Phys. Rev. B 55 (1997) 7014–7017.
[41] T. Sekiya, S. Ohta, S. Kamei, M. Hanakawa, S. Kurita, J. Phys. Chem. Solids 62 (2001) 717–721.
[42] W. Ma, Z. Lu, M. Zhang, Appl. Phys. A 66 (1998) 621.
[43] T. Ohsaka, Solid State Commun. 30 (1979) 345.
[44] L.E. Depero, L. Sangaletti, B. Atlierc, E. Bontempi, A. Marino, M. Zocehi, J. Cryst. Growth 198–199 (1999) 516–520.